Phys Chem Minerals (1988) 15:370–382

PHYSICS AND CHEMISTRY OF MINERALS

A Silicon-29 Nuclear Magnetic Resonance Study of Silicon-Aluminum Ordering in Leucite and Analcite

J.B. Murdoch[1], J.F. Stebbins[2], I.S.E. Carmichael[3], and A. Pines[4]

[1] Picker International, Inc., NMR Clinical Science Center, 5500 Avion Park Drive, Highland Heights, OH 44143, USA
[2] Department of Geology, Stanford University, Stanford, CA 94305, USA
[3] Department of Geology, University of California, Berkeley, CA 94720; and Earth Sciences Division, Lawrence Berkeley Laboratory, Berkeley, CA 94720, USA
[4] Department of Chemistry, University of California, Berkeley, CA 94720; and Materials and Molecular Research Division, Lawrence Berkeley Laboratory, Berkeley, CA 94720, USA

Abstract. Silicon-29 magic-angle-spinning NMR spectroscopy has been used to investigate the silicon-aluminum distribution in natural samples of analcite and leucite (before and after heat treatment) as well as a leucite synthesized from a gel. Three different simulation programs have been developed to fit the experimental spectra. For two we assume a different aluminum occupancy fraction g_i for each of the three crystallographically distinct tetrahedral sites T_i in leucite and some degree of aluminum avoidance, but an otherwise random arrangement of tetrahedral cations. A third program interchanges Al and Si cations on a lattice of $3 \times 3 \times 3$ unit cells to generate an optimized fit. All models predict that the T_2 sites in natural leucite are deficient in aluminum: $g_1 \approx 0.39$, $g_2 \approx 0.16$, and $g_3 \approx 0.42$ for the fractional Al occupancy at each site, with apparently strict aluminum avoidance. Heat treatment of the sample at 1673 K for a week has little effect on the g_i values but may create some Al–O–Al linkages. In the gel-synthesized leucite, Al occupancies are slightly more uniform than in natural leucite: $g_1 \approx 0.36$, $g_2 \approx 0.20$, and $g_3 \approx 0.42$.

For analcite, two distinctly different Si, Al distributions are obtained: (A) $g_1 = g_3 \approx 0.09$, $g_2 \approx 0.78$ and (B) $g_1 = g_3 \approx 0.46$, $g_2 \approx 0.04$. Additional NMR measurements on an ion-exchanged sample or an accurate determination of unit-cell dimensions could resolve this ambiguity.

Introduction

In a previous paper (Stebbins et al. 1986), we described the use of silicon-29 *nuclear magnetic resonance* (NMR) spectroscopy to study defects and short-range order in nepheline group minerals. Here we apply the same technique to investigate the distribution of silicon and aluminum atoms in a second class of feldspathoid minerals, developing in the process several computational methods to find distributions that best match experimental spectra. Phase transitions in most of the samples we will discuss have also been examined recently using differential scanning calorimetry (Lange et al. 1986).

Leucite ($KAlSi_2O_6$) and analcite ($NaAlSi_2O_6 \cdot H_2O$) are silica-poor alkali aluminosilicates with the same topological arrangement of tetrahedral cations. As in feldspars, zeolites, and the silica polymorphs, the tetrahedra – SiO_4 or AlO_4 – form a three-dimensional network structure, with every tetrahedron connected to four others. X-ray and neutron diffraction measurements on single crystals of these minerals (e.g. Taylor 1930; Peacor 1968; Ferraris et al. 1972; Mazzi et al. 1976; Mazzi and Galli 1978) can be used to determine the average coordinates of the tetrahedral sites in the unit cell. However, because diffraction techniques inherently measure long-range averages, determining the true local distribution of silicon and aluminum atoms among these sites is often not possible. In particular, short-range disorder often cannot be distinguished from long-range disorder that results from domain structure.

In contrast, NMR provides a direct, complementary look at short-range structure: a nucleus with non-zero spin is used as a probe of its local electronic environment. As pioneered by Lippmaa et al. (1980, 1981), ^{29}Si magic-angle-spinning (MAS) NMR has been of particular use in the study of silicate minerals. The isotropic chemical shift δ sensitively reflects the bonding environment of a silicon nucleus, varying systematically with several local structural variables. In tectosilicates, the most important of these are the average inter-tetrahedral bond angle Si–O–T (Smith and Blackwell 1983; Thomas et al. 1983; Ramdas and Klinowski 1984) and the number of aluminum next-nearest neighbors. Because of the latter effect, ^{29}Si MAS NMR has been of crucial importance in determining the short-range (and hence energetically most important) distribution of Al and Si in tectosilicates, particularly zeolites (e.g. Lippmaa et al. 1981; Fyfe et al. 1983).

Aluminum-27 MAS NMR at high magnetic fields can also be used to study the distribution of Al among tetrahedral sites in leucite (Phillips and Kirkpatrick 1986). Future combination of the two types of data may eventually lead to improved models for feldspathoid structure.

Sample Characterization

We have examined three samples of natural leucite (one before and after heat treatment), one natural analcite specimen, and a synthetic leucite. Compositional data for the leucite samples, mostly based on electron microprobe measurements, have been presented by Lange et al. (1986). The associated silicon-to-aluminum ratios are listed in Table 1. Powder diffraction data on all samples confirmed that they

Table 1. Silicon-to-aluminum ratios from chemical analysis of leucite and analcite samples[a, b]

	Mt. Cimini leucite	Heat-treated Mt. Cimini leucite	Roccamonfina leucite	Wyomingite leucite	Gel-synthesized leucite[c]	Analcite
Si/Al ratio	2.05	2.02	2.06	2.35	2.09	2.13

[a] Leucite analyses from Lange et al. (1986)
[b] Electron microprobe data, except where noted
[c] Wet chemical data

were pure, and for the synthetic phase, that the desired product was obtained.

Two samples were obtained from leucite-rich volcanic rocks in the Roman District, Italy: the first (labeled "89-21" in Lange et al. 1986) from Mt. Cimini, the second (University of California, Berkeley, Department of Geology and Geophysics, collection number 16682; labeled "90-05" by Lange et al.) from Roccamonfina. Each is close in composition to the ideal stoichiometry $KAlSi_2O_6$, and the two samples yielded very nearly identical ^{29}Si MAS NMR spectra. These were analyzed separately, but also were averaged together to improve the overall signal-to-noise ratio and thus minimize the effect of artifacts in deconvolution and simulation. The combination will be referred to as "natural leucite." In addition, to study thermal effects on Si, Al ordering, a portion of the Mt. Cimini sample was heat treated at 1673 K for one week.

The third leucite sample (labeled "1774" in Lange et al. 1986), which exhibits no optically observable twinning, is from the groundmass of a wyomingite lava obtained, appropriately enough, in the Leucite Hills of Wyoming (Carmichael 1967). It contains 2.3 weight percent Fe and has a higher Si/Al ratio (2.35) than the other feldspathoid samples we have examined.

To investigate the effect of excess SiO_2 in solid solution, a synthetic leucite was prepared as a gel using the technique of Hamilton and Henderson (1968), then dehydrated and heated in a Pt crucible for 3 days at 1373 K, followed by 5 days at 1773 K (Lange et al. 1986, sample SL. 2). Electron microprobe and wet chemical data indicate that the product is approximately 86 weight percent $KAlSi_2O_6$ and 14 weight percent $KAlSi_3O_8$.

The analcite sample is in the form of colorless needles from Golden, Colorado (composition by weight from electron microprobe data: 56.8 percent SiO_2, 22.7 percent Al_2O_3, and 14.1 percent Na_2O, with 8.0 percent H_2O specified). A portion of this sample was dehydrated for 23 h at 1033 K. In turn, part of the dehydrated sample was used to create a potassium-exchanged analcite by heating it in molten KBr at 1033 K for 44 h. This procedure is not expected to affect the distribution of Al and Si cations (Waldbaum and Robie 1971). Intriguingly, however, the resulting leucite gave no ^{29}Si NMR signal. The likely reasons for this lack of response will be discussed later.

Experimental Details

As in previous work (Stebbins et al. 1986), spectra were obtained on a "home-built" Fourier transform NMR spectrometer operating at 8.5 tesla with a magic-angle-spinning probe from Doty Scientific. Powdered samples were spun in alumina rotors at 2.5–3.5 kHz, and spinning sideband peaks were small for all samples except the wyomingite leucite.

From 660 to 8300 free induction decays were acquired and averaged together for each spectrum. The rf pulse tip angle was approximately 45°, and successive pulses were spaced at 4–120 seconds to avoid spectral distortion resulting from incomplete spin-lattice (T_1) relaxation. Silicon chemical shifts were measured relative to an external sample of tetramethylsilane or relative to a secondary standard: a spinning sample of crystalline jadeite ($NaAlSi_2O_6$, $\delta = -92.0$ ppm). Except for the case of analcite, dehydrated analcite, and wyomingite leucite, no modification (other than truncation) of free induction decay signal was performed prior to Fourier transformation. Triangular apodization of these data gave rise to an increase in linewidth of at most a few percent.

Isotropic lineshapes have been deconvoluted and simulated using a number of programs described in a later section. For all analyzed spectra, however, the small spinning sideband lineshapes have not been included in the deconvolution process: their lower signal-to-noise ratio plus some roll in the baseline preclude a quantitative multi-component fit. Omission of the sidebands introduces some error in the relative peak areas for each silicon type, which in turn affects the structural interpretation. However, we believe that this source of error can be neglected relative to the uncertainties in deconvolution of the center peaks. Except in the case of the wyomingite leucite (which was only examined qualitatively), no sideband is more than roughly 15 percent as high as the corresponding center peak. Moreover, the sideband lineshapes, when distinguishable, are miniature versions of the center peaks, suggesting that, as one might expect, chemical shift anisotropies associated with the different silicon sites do not vary widely. Hence center peak areas are probably scaled down uniformly relative to total peak areas.

Structural Considerations

Before discussing the NMR spectra we have obtained, a closer look at the connectivity of tetrahedral cations in leucite minerals is necessary. There are 48 tetrahedral sites in the unit cell, which is cubic (or nearly so) for analcite and tetragonal for leucite itself. Galli et al. (1978) have presented an elegant model for visualizing the intricate tetrahedral framework. As noted also by Merlino (1984), the building block for this idealized structure can be considered to be a square prism with two of the long edges missing. The structure of a unit cell is shown in Figure 1, a view looking approximately along the c-axis. The circles represent tetrahedral cations (Al or Si), and intervening oxygens are omitted. Three sets of the aforementioned prisms can

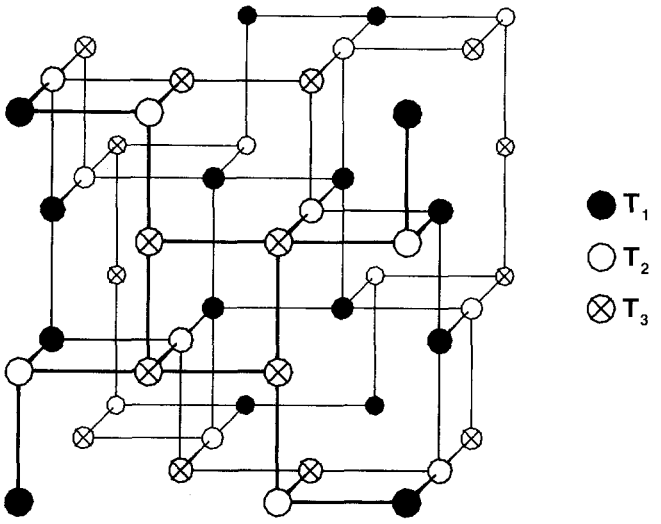

Fig. 1. An idealized unit cell for leucite group minerals that illustrates the connectivity of the 48 tetrahedral sites. Circles represent tetrahedral cations (Si or Al) and oxygens are omitted. The view is approximately along the *c*-axis, and the three types of crystallographically distinct T_i sites in low-temperature leucite (space group $I4_1/a$) are displayed

be seen, each set oriented parallel to one of the unit cell axes. The three sets of crystallographically distinct tetrahedral sites T_i for low temperature leucite ($I4_1/a$ symmetry) are also apparent. Each tetrahedral node is part of two four-membered rings (end pieces of the prisms) and two six-membered rings (which appear chair-shaped in this representation). Not shown are the two types of interstitial sites occupied by charge-balancing alkali cations or water molecules: the so-called S sites, located at the center of each prism, and the W sites, located midway along the missing edges of each prism. There are 24 S sites and 16 W sites per unit cell (Galli et al. 1978).

The topologic symmetry (Smith 1982) of the unit cell in Figure 1 is cubic: $Ia3d$, with all tetrahedral sites equivalent. Assuming a random arrangement of tetrahedral cations Al and Si, the topochemical symmetry (a long-range average over a multitude of unit cells) is also $Ia3d$. However, a mismatch in the size of the extra-framework species present can induce structural distortion and lower the real symmetry. In pollucite [a naturally occurring cesium analog (Beger 1969)], large Cs^+ ions (and water molecules in some samples) occupy the W sites, and the overall cubic symmetry is maintained. In analcite, $NaAlSi_2O_6 \cdot H_2O$, water molecules occupy the W sites and sodium ions occupy two-thirds of the S sites (Galli et al. 1978). Its structure has also been characterized as cubic (Taylor 1930; Ferraris et al. 1972), but more recent work (Mazzi and Galli 1978) indicates that small deviations can exist and that the real symmetry is lower. Some samples were found by these authors to be tetragonal: $I4_1/acd$, with sites T_1 and T_3 in Figure 1 equivalent and either $c > a$ or $a > c$. Others were found to be orthorhombic ($Iabc$).

In leucite, potassium ions occupy the W sites and the S sites are vacant. Above roughly 900 K, the symmetry is $Ia3d$ as in pollucite (Peacor 1968). At lower temperatures, however, because K^+ is smaller than either Cs^+ or H_2O, the framework structure collapses around the potassium ions to maintain a favorable K–O distance. The tetragonal symmetry that results is $I4_1/a$, with $a = 13.09$ Å, $c = 13.75$ Å (Mazzi et al. 1976). The characteristic four-fold screw axes parallel to the *c*-axis are apparent in Figure 1.

Inversion from the high-temperature cubic phase to the low-temperature tetragonal phase also gives rise to extensive merohedric and pseudomerohedric twinning (Mazzi et al. 1976). However, because MAS NMR is a probe of short-range structure, the presence of twinning will have an effect on the leucite ^{29}Si spectrum only if silicons on the twin boundaries are a measurable fraction (at least one percent) of the total number of silicons present and if these silicons have a different chemical shift as a result of site distortion.

One may note that there are three varieties of four-membered rings in the leucite structure: one with four T_1 sites, one with four T_3 sites, and one composed of two T_2 sites, a T_1 site, and a T_3 site. The sites themselves can be further distinguished as follows:

Each T_1 site has two T_1 neighbors and two T_2 neighbors.
Each T_2 site has two T_1 neighbors and two T_3 neighbors.
Each T_3 site has two T_2 neighbors and two T_3 neighbors.

Because the chemical shift of a silicon-29 nucleus depends on the identity – Si or Al – of adjacent tetrahedral cations, such connectivity information is crucial for interpreting the NMR lineshape and determining the nature of Si, Al ordering.

With this background, we can now examine how silicon and aluminum are distributed on the lattice of tetrahedral sites. Single-crystal x-ray diffraction results suggest that the arrangement is completely random in leucite; in analcite, random but with enrichment of Al in one type of site and Si in the other, depending on the ratio of unit-cell dimensions (Galli et al. 1978).

NMR data provide information directly on local cation distributions. In particular, previous work on a wide variety of alkali aluminosilicates, including other feldspathoids (Stebbins et al. 1986), has demonstrated that in these materials, one constraint on tetrahedral cation disorder is of general validity: the aluminum-avoidance principle or "Loewenstein's rule" (Loewenstein 1954). This principle states that energetically unfavorable Al–O–Al linkages do not occur in aluminosilicates for which the Si/Al ratio is greater than or equal to one. It appears to be true even for $NaAlSiO_4$ (carnegieite) synthesized at 1673 K and for volcanic nepheline ([Na, K] $AlSiO_4$) (Stebbins et al. 1986). We will therefore assume that some degree of aluminum avoidance is present in our analysis of leucite and analcite. (As will be shown, our data are indeed consistent with this assumption.)

Tectosilicates with network-modifying cations smaller or more highly charged than Na^+ or K^+ may show greater disorder, including Al–O–Al bonds, when prepared at high temperature or under disequilibrium conditions. The reasons for this difference are discussed below.

Results

Analcite

Figure 2 displays the ^{29}Si MAS NMR spectrum of analcite; peak positions, widths, and areas are listed in Table 2. Because the tetrahedral sites $T_1 = T_3$ and T_2 are very nearly equivalent (as evidenced in part by the Si–O–T angles listed below), ^{29}Si chemical shifts are a function only of the number of aluminum neighbors – there is no "intrinsic"

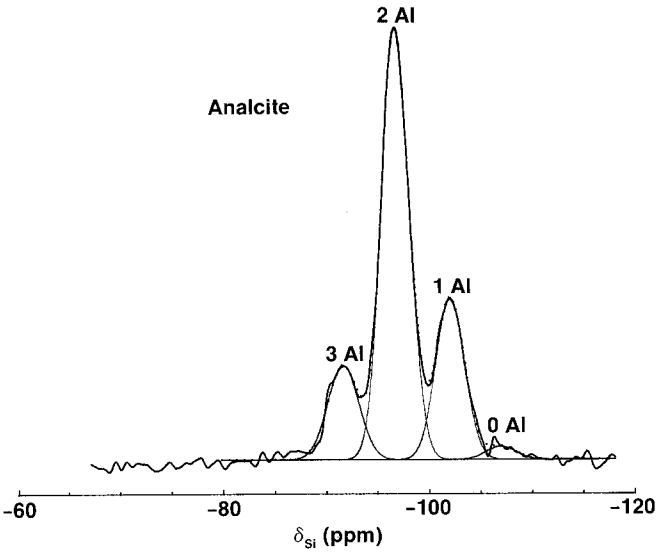

Fig. 2. The ^{29}Si MAS NMR spectrum of analcite (1259 acquisitions with a recycle time – the interval between successive rf pulses – of 40 s). The chemical shift δ is given in ppm relative to a tetramethylsilane standard. In this and subsequent spectra, the thick solid line is the experimental lineshape, the thin solid lines delineate individual Gaussian components, and the dotted line is the sum of these deconvoluted peaks. The small spinning sidebands are not shown; they lie beyond the range of this plot

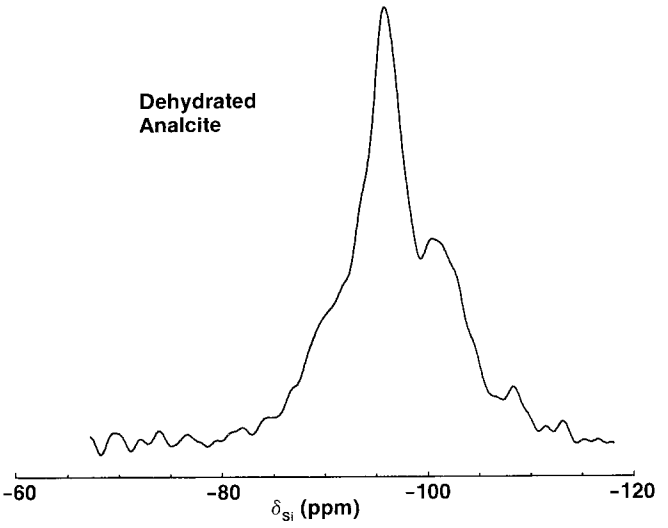

Fig. 3. The ^{29}Si MAS NMR spectrum of dehydrated analcite (662 acquisitions, 120 s recycle time)

Table 2. Deconvolution of the analcite spectrum into Gaussian components

Peak	Chemical shift (ppm)	FWHM[a] (ppm)	Relative area (%)	Number of Al neighbors
1	− 91.6	3.5	14.8±0.3	3
2	− 96.8	3.1	59.7±0.3	2
3	−102.0	3.3	23.4±0.3	1
4	−106.9	3.4	2.0±0.3	0

[a] Full width at half-maximum of the Gaussian component

shift difference between sites. Hence each peak in Figure 2 corresponds to silicons with a fixed number of Si−O−Al linkages.

Peak assignments can be made using one of several empirical formulas that relate δ_{Si} to particular structural parameters. For example, Ramdas and Klinowski (1984) have found that δ_{Si} in tectosilicates can be expressed as the sum of a constant term, a term proportional to the average distance to adjacent tetrahedral cations (expressed in terms of θ, the average Si−O−T bond angle), and an electrostatic deshielding term proportional to k, the number of Al neighbors. Combining their Equations 1 and 2 yields the following relationship:

$$\delta = 143.03 - (263.61 + 2.64k) \sin \theta/2 + 7.95k. \quad (1)$$

As such, δ can be written as a zero-aluminum-neighbor shift $\delta(0\text{Al})$ plus k times a shift increment $\Delta\delta$. Using bond angles obtained by Mazzi and Galli (1978) for seven different analcite samples, one finds $\theta(T_1) = 144.3° \pm 0.2°$ and $\theta(T_2) = 144.5° \pm 0.4°$, where standard deviations are indicated. From Equation 1, the average deviation between $\theta(T_1)$ and $\theta(T_2)$ of 0.3° corresponds to an estimated chemical shift difference of at most 0.2 ppm. Hence for both sites, $\delta(0\text{Al}) = -108.0$ ppm, $\delta(1\text{Al}) = -102.5$ ppm, $\delta(2\text{Al}) = -97.1$ ppm, $\delta(3\text{Al}) = -91.7$ ppm, $\delta(4\text{Al}) = -86.2$ ppm, and $\Delta\delta = 5.44$ ppm. These estimated chemical shifts are in good agreement with experimental values and substantiate the peak assignments in Figure 2 and Table 2. Note that there are apparently no silicons present with four Al neighbors. The silicon-to-aluminum ratio R can be obtained from the relative peak areas I_k. The average number of aluminum neighbors per silicon is given by

$$\langle k \rangle = \Sigma k I_k / \Sigma I_k; \quad (2)$$

if Loewenstein's rule is obeyed,

$$R = 4/\langle k \rangle \quad (3)$$

(Klinowski et al. 1982). Using the peak areas for analcite, one finds $\langle k \rangle = 1.87$ and $R = 2.14$, in excellent agreement with the electron microprobe measurement listed in Table 1. Were a substantial number of Al−O−Al linkages present, the value of R obtained using Equation 3 would be considerably larger than the microprobe result. We will return to the analysis of analcite peak areas in a later section.

The ^{29}Si MAS NMR spectrum of an analcite sample dehydrated at 1033 K for 23 hours is displayed in Figure 3. The absence of water molecules in the W sites has apparently distorted the tetrahedral framework, broadening the peaks associated with each type of silicon present and increasing the overall range of chemical shifts. Because the spectrum lacks distinct "bumps" and shoulders, however, we have not attempted to deconvolute it into a sum of Gaussian components.

As stated earlier, we also prepared a potassium-exchanged dehydrated analcite that unfortunately gave rise to no measurable ^{29}Si NMR signal. We believe that this lack of response is a consequence of an extremely long ^{29}Si spin-lattice relaxation time T_1:[T_1 is the characteristic time for nuclear spin state populations to return to their equilibrium values (following rf pulse perturbation) via energy exchange with their surroundings.] Indeed, there is a likely reason why T_1 (not to be confused with the tetrahedral

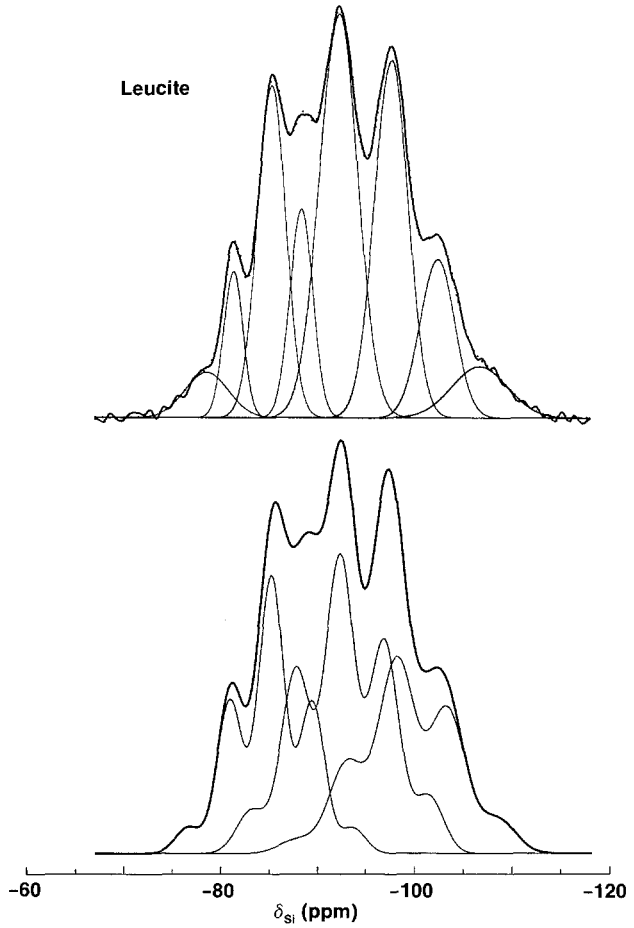

Fig. 4. (top) A weighted sum of ^{29}Si MAS NMR spectra for the Mt. Cimini and Roccamonfina leucite samples (Mt. Cimini leucite: 1077 acquisitions, 40 s recycle time +2000 acquisitions, 5 s recycle time; Roccamonfina leucite: 2647 acquisitions, 15 s recycle time). (bottom) Model 3 lineshape simulation. T_3, T_2, and T_1 subspectra appear from left to right

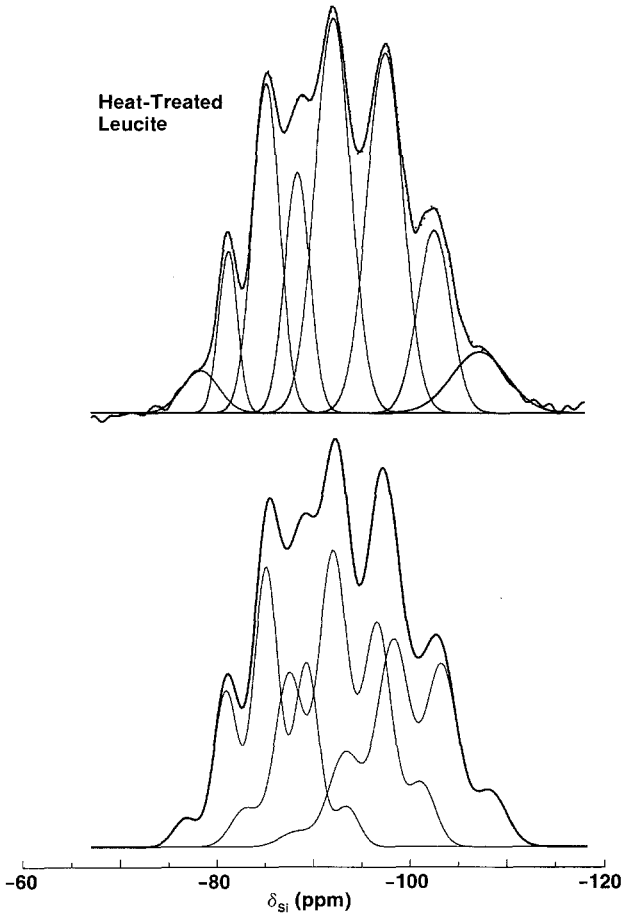

Fig. 5. The ^{29}Si MAS NMR spectrum of the heat-treated Mt. Cimini leucite sample (1501 acquisitions, 20 s recycle time +4292 acquisitions, 15 s recycle time +2500 acquisitions, 4 s recycle time), plus a model 3 simulation

site designation) should be longer in our potassium-exchanged analcite than in the untreated original sample. In non-porous silicates, the predominant coupling pathway between nuclear spin states and the lattice is via the unpaired electrons in paramagnetic impurities, e.g. Fe^{2+} or Fe^{3+} ions (Barron et al. 1983). [Nuclei near the paramagnetic species relax rapidly; adjacent nuclei in an expanding shell are then relaxed by a process known as spin diffusion: an energy-conserving "flip-flop" of nuclear states (Abragam 1961).] The concentration of paramagnetic ions, low to begin with in our microprobe standard analcite specimen, was no doubt further reduced in the high-temperature ion exchange process. The resulting impurity concentration was apparently less than in our gel-synthesized leucite sample, for which a spectrum was readily obtained.

A second mechanism that could account for the apparent increase in silicon T_1 after ion exchange is a relaxation pathway involving dipole-dipole coupling between ^{29}Si and quadrupolar ^{23}Na nuclei (100% isotopic abundance). Potassium-39 (93.1% abundant) is also a quadrupolar nucleus, but interacts less strongly with ^{29}Si than does ^{23}Na because its gyromagnetic ratio is smaller by a factor of 5.67. The same substitional effect on T_1 has been seen in nepheline minerals (Stebbins et al. 1986) and in alkali silicate glasses (Schneider et al. 1987).

Leucite

The averaged ^{29}Si MAS NMR spectrum obtained for the Mt. Cimini and Roccamonfina leucite samples is displayed in Figure 4. The lineshape was not appreciably altered by varying the delay between successive rf pulses from 5 to 40 s, suggesting that all the silicons present have roughly the same spin-lattice relaxation time. The spectrum of the heat-treated Mt. Cimini leucite sample appears in Figure 5 and that of the gel-synthesized leucite in Figure 6.

Peak assignments and the analysis of intensities will be discussed in the next section. We note here, however, that heat treatment of leucite at 1673 K for a week has at most a small effect on its ^{29}Si NMR spectrum and hence on the nature of its short-range Si, Al order. As observed by differential scanning calorimetry, heat treatment did lower the tetragonal-cubic phase transition temperature by 24° and better resolved two peaks on the heat capacity curve (Lange et al. 1986). We should also note that prior to quantitatively deconvoluting the leucite spectrum on the computer, we incorrectly described it in a preliminary report as a series of sharp peaks centered on a broad background absorption (Murdoch et al. 1984).

The wyomingite leucite spectrum is shown in Figure 7. Because of the low signal-to-noise ratio, no peak fitting

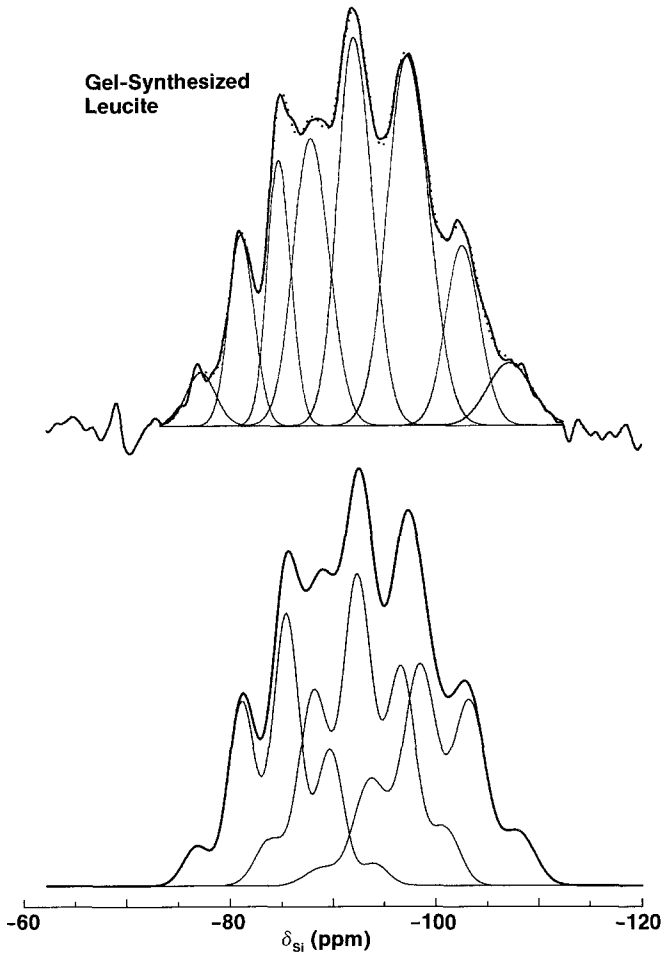

Fig. 6. The ^{29}Si MAS NMR spectrum of gel-synthesized leucite (1716 acquisitions, 40 s recycle time), plus a model 3 simulation

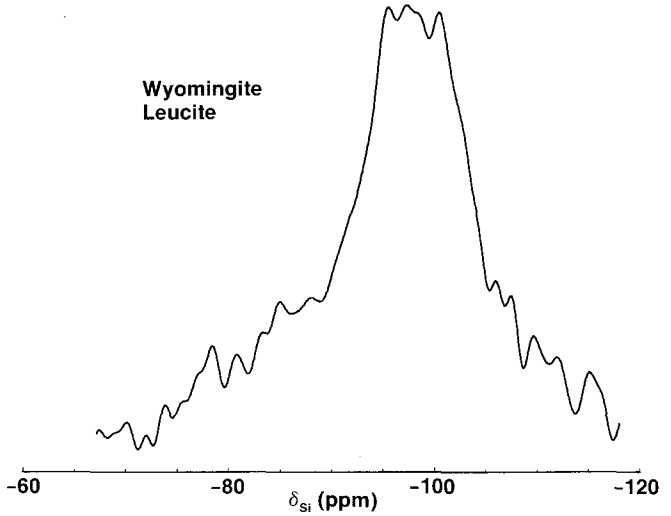

Fig. 7. The ^{29}Si MAS NMR spectrum of wyomingite groundmass leucite (316 acquisitions, 30 s recycle time +758 acquisitions, 60 s recycle time)

was attempted, but it is apparent that a distinctly different Si, Al distribution must exist in this sample than in the other leucites. In addition, as mentioned earlier, spinning sidebands for this sample are noticeably larger. This sideband enhancement is the result of an anisotropic coupling

Table 3. Deconvolution of the leucite spectra into Gaussian components

Sample	Peak	Chemical shift (ppm)	FWHM (ppm)	Relative area (%)
Natural leucite	1	− 78.7	5.2	3.6±0.2
	2	− 81.4	2.3	5.1±0.2
	3	− 85.3	3.4	17.2±0.3
	4	− 88.4	2.8	8.7±0.4
	5	− 92.2	4.6	28.2±0.5
	6	− 97.6	4.1	21.9±0.3
	7	−102.3	4.2	10.0±0.5
	8	−106.7	6.7	5.2±0.4
Heat-treated leucite	1	− 78.4	4.4	2.7±0.1
	2	− 81.3	2.3	5.4±0.1
	3	− 85.2	3.3	16.0±0.3
	4	− 88.4	3.0	10.8±0.5
	5	− 92.1	4.3	25.1±0.5
	6	− 97.5	4.4	23.2±0.3
	7	−102.5	4.0	10.7±0.3
	8	−107.2	6.7	6.0±0.3
Gel-synthesized leucite	1	− 77.3	3.3	2.6±0.1
	2	− 81.3	2.9	8.0±0.1
	3	− 85.0	2.7	10.3±0.5
	4	− 88.1	4.1	17.1±1.0
	5	− 92.4	3.9	22.2±0.6
	6	− 97.5	4.7	25.3±0.4
	7	−102.7	3.8	10.0±0.3
	8	−107.2	5.0	4.5±0.3

to the unpaired electrons associated with the 2.3 weight percent iron present. The same effect has been seen in glasses prepared from silicic lavas (Murdoch et al. 1985).

Interpretation of the Leucite Spectra

Overview

Our goal is to use relative peak areas from deconvolution and lineshape simulation programs to determine the distribution of silicon and aluminum cations among the different T_i sites. Similar analyses have been published recently for cordierite (Putnis et al. 1985; Putnis and Angel 1985) and synthetic mazzite (Jarman et al. 1984; Klinowski and Anderson 1986).

The first step is peak assignment. There are three inequivalent tetrahedral sites in low-temperature leucite, and for each a silicon can have 0 to 4 aluminum neighbors. Hence there can exist 15 different silicon species. Were 15 distinct peaks present in the leucite spectrum, our task would be relatively straightforward. However, each of the three experimental lineshapes in Figures 4–6 appears to be made up of only eight peaks or shoulders.

To quantify this observation, we have deconvoluted each spectrum using a modification of a peak-fitting program originally developed for Raman spectra (Mysen et al. 1982). Individual peaks are assumed to be Gaussian, mirroring the statistically normal distribution of bond length and bond angle values expected in a disordered crystal. We limit the number of components in the lineshape-fitting process to eight, then let the program freely vary the position, height, and width of each component to obtain an optimal fit. The output, as listed in Table 3, includes an estimated

Table 4. Estimated chemical shifts for $T_i(k\,\mathrm{Al})$ silicon species in leucite[a]

	T_1 sites	T_2 sites	T_3 sites
Average Si−O−T angle[b]	145.9°	138.9°	130.4°
δ_{Si} (ppm) for			
0 Al	−109.0	−103.8	−96.3
1 Al	−103.5	− 98.3	−90.7
2 Al	− 98.1	− 92.9	−85.2
3 Al	− 92.7	− 87.4	−79.6
4 Al	− 87.3	− 81.9	−74.1
$\Delta\delta$ (ppm)	5.43	5.48	5.55

[a] Calculated using Equation 1, a relationship derived by Ramdas and Klinowski (1984)
[b] From bond angles obtained by Mazzi et al. (1976)

standard deviation for each peak area; these values are incorporated in subsequent structural analysis.

To interpret the results, we again turn to the linear relationship between δ_{Si} and the average Si−O−T bond angle expressed in Equation 1. Using bond angles calculated from single-crystal x-ray diffraction data by Mazzi et al. (1976), we can estimate the chemical shift for each of the 15 silicon species, as listed in Table 4. Note that the estimated intrinsic shift between T_1 (0 Al) and T_3 (0 Al) silicons is 12.7 ppm, a larger intrinsic shift than has been seen in zeolites. Note also that the average Si−O−T bond angle for site T_1 is nearly the same as that for all tetrahedra in analcite. We expect, therefore, that T_1 silicons contribute to the four leucite peaks (5–8) that coincide with peaks in the analcite spectrum.

The estimated leucite chemical shifts provide a starting point for detailed structural analysis, for which we have used three different computer modeling techniques. With models 1 and 2, each of the 15 possible Si species is matched to one of the eight deconvoluted experimental peaks (or is assumed to be nonexistent). This approach entails some sort of peak assignment scheme; four examples are listed in Table 5. The relative merits of these will be discussed below. Model 1 assumes a different aluminum occupancy value for each of the three T_i sites and the existence of some degree of aluminum avoidance, but an otherwise random distribution of Al and Si. Model 2 begins with an initial distribution of Al and Si on a $3 \times 3 \times 3$-unit-cell lattice of sites, then generates random Al jumps (subject to aluminum avoidance) to obtain a progressively better fit to the eight experimental peak areas.

The third model we have developed does not make use of the eight deconvoluted Gaussians. Instead, the entire leucite lineshape is simulated as the sum of 15 peaks, subject to a number of constraints on intensity, linewidth, and position. Because it avoids the all-or-nothing nature of peak assignments, we feel that this model is the most reliable. However, we present results for all three to demonstrate that *our basic findings are not tied to a single simulation scheme.* Each model is described in more detail below.

Model 1

Assume we have N T_1 sites, N T_2 sites, and N T_3 sites with the connectivity of the leucite lattice, where N is the proverbial large number. These give rise to N T_1-T_1 bonds (omitting the intervening oxygens), N T_3-T_3 bonds, $2N$ T_1-T_2 bonds, and $2N$ T_2-T_3 bonds, but no T_1-T_3 or T_2-T_2 bonds. Let g_1, g_2, and g_3 be the fraction of each type of site occupied by aluminum. If we define

$$\langle g\rangle=(g_1+g_2+g_3)/3, \tag{4}$$

then the Si/Al ratio is given by

$$R=\frac{1-\langle g\rangle}{\langle g\rangle}. \tag{5}$$

In order to quantify the degree of aluminum avoidance, let α represent the average propensity for Al−Al linkages to form: $\alpha=0$ corresponds to strict Al avoidance; $\alpha=1$ signifies that Al−O−Al bonds are no different from Si−O

Table 5. Leucite peak assignment schemes

Peak	Scheme I	Scheme II
1	T_3(4 Al)	T_3(4 Al)
2	T_3(3 Al)	T_3(3 Al)
3	T_2(4 Al) + T_3(2 Al)	T_3(2 Al)
4	T_1(4 Al) + T_2(3 Al) + T_3(1 Al)	T_1(4 Al) + T_2(4 Al) + T_3(1 Al)
5	T_1(3 Al) + T_2(2 Al) + T_3(0 Al)	T_1(3 Al) + T_2(3 Al) + T_3(0 Al)
6	T_1(2 Al) + T_2(1 Al)	T_1(2 Al) + T_2(2 Al)
7	T_1(1 Al) + T_2(0 Al)	T_1(1 Al) + T_2(1 Al)
8	T_1(0 Al)	T_1(0 Al) + T_2(0 Al)

Peak	Scheme III	Scheme IV
1	T_2(4 Al)	T_3(3 Al)
2	T_3(3 Al)	T_3(2 Al)
3	T_1(4 Al) + T_2(3 Al)	T_3(1 Al)
4	T_3(2 Al)	T_1(4 Al) + T_2(4 Al) + T_3(0 Al)
5	T_1(3 Al) + T_2(2 Al) + T_3(1 Al)	T_1(3 Al) + T_2(3 Al)
6	T_1(2 Al) + T_2(1 Al) + T_3(0 Al)	T_1(2 Al) + T_2(2 Al)
7	T_1(1 Al) + T_2(0 Al)	T_1(1 Al) + T_2(1 Al)
8	T_1(0 Al)	T_1(0 Al) + T_2(0 Al)

Table 6. Model 1 simulation values for aluminum T_i site occupancies in leucite[a]

Sample	Assignment scheme	g_1	g_2	g_3	R	α	Relative rms error (%)
Natural leucite	I	0.41	0.09	0.50	2.00	[0.0]	18.9
	II	0.50	0.17	0.42	1.75	[0.0]	20.6
	III	0.45	0.17	0.41	1.91	[0.0]	15.7
	IV	0.50	0.18	0.25	2.23	[0.0]	23.9
	I	0.40	0.09	0.49	[2.06]	0.0	19.1
Heat-treated leucite	I	0.39	0.11	0.46	2.13	[0.0]	13.8
	I	0.39	0.11	0.48	[2.06]	0.12	13.7
Gel-synthesized leucite	I	0.34	0.26	0.38	2.06	[0.0]	8.7
	I	0.33	0.28	0.36	[2.09]	0.0	8.9

[a] Fixed values for R or α are indicated by square brackets

$-$Si or Si$-$O$-$Al bonds. The number of Al$-$Al linkages present is consequently as follows:

$N\alpha g_1^2$ Al[T_1] to Al[T_1] bonds,
$2N\alpha g_1 g_2$ Al[T_1] to Al[T_2] bonds,
$2N\alpha g_2 g_3$ Al[T_2] to Al[T$_3$] bonds,
$N\alpha g_3^2$ Al[T_3] to Al[T_3] bonds.

In turn, recognizing that each Al$-$Al linkage eliminates two Si$-$Al linkages, we can list the total number of Si$-$Al bonds:

$(2Ng_1-2N\alpha g_1^2)$ Si[T_1] to Al[T_1] bonds,
$(2Ng_1-2N\alpha g_1 g_2)$ Si[T_2] to Al[T_1] bonds,
$(2Ng_2-2N\alpha g_1 g_2)$ Si[T_1] to Al[T_2] bonds,
$(2Ng_2-2N\alpha g_2 g_3)$ Si[T_3] to Al[T_2] bonds,
$(2Ng_3-2N\alpha g_2 g_3)$ Si[T_2] to Al[T_3] bonds,
$(2Ng_3-2N\alpha g_3^2)$ Si[T_3] to Al[T_3] bonds.

The *probability* of each is found by dividing the number of bonds from Si[T_i] to Al[T_j] by the *total* number of bonds from Si[T_i] to a T_j site:

$$P(i,j)=\frac{2Ng_j(1-\alpha g_i)}{2N(1-g_i)}=\frac{g_j(1-\alpha g_i)}{1-g_i}. \tag{6}$$

In turn, the probability of a Si[T_i] to Si[T_j] bond is given by

$$Q(i,j)=1-P(i,j). \tag{7}$$

Note that to keep probabilities greater than or equal to zero and less than or equal to one, we must have

$$g_1, g_3 \leqq \frac{1}{1+(1-\alpha)^{1/2}}, \tag{8a}$$

$$g_2 \leqq \frac{1-g_1}{1-\alpha g_1}, \tag{8b}$$

$$g_2 \leqq \frac{1-g_3}{1-\alpha g_3}. \tag{8c}$$

The limits vary according to the level of aluminum avoidance.

To further compress notation, we now relabel the following single-bond aluminum-neighbor probabilities: $a_1=P(1,1)$, $b_1=P(1,2)$, $a_2=P(2,1)$, $b_2=P(2,3)$, $a_3=P(3,2)$, and $b_3=P(3,3)$. In addition, we define analogous Si-neighbor probabilities: $c_i=1-a_i$ and $d_i=1-b_i$. To obtain an expression for $n_i(k)$, the number of silicons in site T_i with k adjacent Al cations, we must multiply the population of silicons in site T_i, $N(1-g_i)$, by the probability of their having k Al neighbors. This probability is given by the sum of the probabilities for different Al arrangements:

$$n_i(4)=N(1-g_i)(a_i^2 b_i^2), \tag{9a}$$

$$n_i(3)=N(1-g_i)(2a_i c_i b_i^2+2a_i^2 b_i d_i), \tag{9b}$$

$$n_i(2)=N(1-g_i)(a_i^2 d_i^2+c_i^2 b_i^2+4a_i c_i b_i d_i), \tag{9c}$$

$$n_i(1)=N(1-g_i)(2a_i c_i d_i^2+2c_i^2 b_i d_i), \tag{9d}$$

$$n_i(0)=N(1-g_i)(c_i^2 d_i^2). \tag{9e}$$

At this point, a computer is used to determine which set of aluminum site occupancy values $\{g_1, g_2, g_3\}$ best matches the experimental peak areas for a particular assignment scheme. An outline of the program is as follows:

(1) Loop over the allowed g_1, g_2, and g_3 values (plus α if it is varied) in increments of 0.01.

(2) For every combination of g_i and α values, calculate the number of silicons in each T_i site with k Al neighbors.

(3) Combine these numbers according to the peak assignment scheme of choice.

(4) Scale the simulated intensities to provide the best weighted-least-squares fit to the experimental peak areas.

(5) Calculate the rms error for each $\{g_1, g_2, g_3, \alpha\}$ combination, and keep track of the "winners."

Before discussing results, we note the following limitation. Because our window into the nature of Si, Al ordering is the ^{29}Si NMR spectrum, what we know of Al$-$Al bonds is indirectly measured. For example, both an increase in the number of Al$-$Al linkages and an increase in the Si/Al ratio have the effect of lowering the total number of Si$-$Al bonds, which in turn changes the distribution of T_i (k Al) silicon species. Indeed, α and R are somewhat interdependent variables, and for model 1, we therefore choose to not let them vary independently.

Results are listed in Table 6 for the Mt. Cimini + Roccamonfina leucite spectrum, analyzed using assignment schemes I–IV, with α set equal to zero and R free to vary from 1.0 to 99.0. Assignment scheme III generates the best rms fit to the experimental peak areas, but scheme I is the most consistent with the electron microprobe Si/Al values found in Table 1. Hence we will focus on scheme I here. Also in Table 6 are data for the heat-treated and gel-synthesized leucites. In all three samples, an inequality exists in the aluminum occupancy of the three T_i sites, with T_3 the

most hospitable to Al cations and T_2 the least so. For natural leucite, the difference in g_i values before and after heat treatment may possibly be a real effect, but is much more likely an indication of the uncertainties in the analysis.

With R fixed at electron microprobe values and α free to vary, we obtain g_i values almost identical to those in Table 6 and find $\alpha = 0.0$, 0.12, and 0.0 for the natural, heat-treated, and gel-synthesized leucites, respectively. Similar numbers are generated using model 3 and are discussed below.

Model 2

As noted earlier, the previous model incorporates a variable Al occupancy for each T_i site and variable aluminum avoidance, but otherwise assumes a random distribution of Al and Si. As a consequence, the relative abundance of various silicon species can be expressed in terms of simple probability relationships. There may exist, however, additional constraints or tendencies that affect the actual Si, Al distribution. An example is Dempsey's rule (Dempsey et al. 1969; Vega 1983), which in generalized form states that for electrostatic reasons, the number of Al–Si–Al linkages should be minimized.

To investigate possible non-random cation distributions (within the bounds of strict Al avoidance, however) and to better fit the experimental peak areas, we have devised a "directed jump" simulational technique, inspired by the method Vega (1983) has used to study adherence to Dempsey's rule in zeolites. Our starting point is a $3 \times 3 \times 3$ array of unit cells with periodic boundary conditions. The 1296 tetrahedral sites (48 in each of the 27 unit cells) constitute a feldspathoid microcosm, one that is meant to be large enough to allow for a wide variety of Si, Al configurations but small enough to be analyzed in a reasonable amount of computer time. In accord with the R value of choice, a semi-random pattern of Al cations is scattered among the tetrahedral sites, which otherwise are assumed to contain silicon. Next an initial set of simulated peak areas is generated, based on the relative number of each type of silicon present and the assignment scheme one has selected. The rms error in fitting the experimental peaks is computed and stored as the current "record." A silicon and an aluminum cation are then selected randomly for a possible swap in position on the lattice. For the swap to be allowed, no violations of the aluminum-avoidance rule can occur, and the resulting set of simulated peak areas must be a better fit to the experimental spectrum. If the move is allowed, the rms error record is also updated. The process continues until selected Si, Al swaps fail to break the error record 1000 times in a row. The entire procedure is then repeated several times in an attempt to obtain the best possible fit for a particular value of R. Finally, in the outermost loop of the program, the input Si/Al ratio itself is varied over a narrow range about its experimentally determined value, again in the quest for an optimum fit. (We chose the increment in Si/Al values to be 0.05.)

Listed in Table 7 are results for "winning" distributions found for each of the three leucite samples. When two different Si/Al ratios produced comparably small rms error values, both data sets are listed. Two observations can be made. First, the aluminum distributions generated by this directed jump simulation are in good agreement with those of model 1 for natural leucite, with and without heat treatment. For the gel-synthesized sample, a more differentiated Al distribution is generated than with model 1, a distribution more like (but not identical to) that found for natural leucite. Second, for all three samples, the quality of the fit, as evidenced by the optimized rms error values, is noticeably improved relative to model 1. Much of this improvement may simply be an adjustment of the calculated Si, Al distribution to mask errors inherent in the peak assignment process. However, a similar, though smaller, improvement in fit for model 2 compared to model 1 is also seen with analcite, for which the peak assignments are unambiguous. Hence there may well be more to the Si, Al distribution in leucites than T_i site preferences and aluminum avoidance.

Table 7. Model 2 simulation values for aluminum T_i site occupancies in leucite

Sample	Si/Al ratio	g_1	g_2	g_3	Relative rms error (%)
Natural leucite	2.05	0.37	0.14	0.48	0.32
Heat-treated leucite	2.10	0.36	0.13	0.48	1.11
	2.15	0.35	0.14	0.46	0.23
Gel-synthesized leucite	2.10	0.36	0.17	0.44	0.46
	2.15	0.36	0.19	0.41	0.28

Model 3

Rather than varying g_i values to match a set of peak areas for each spectrum, we can instead simulate spectral lineshapes directly. In the absence of constraints, this would entail a 45-parameter fit: a Gaussian characterized by height, width, and chemical shift for each of the 15 possible silicon species. However, we have seen that each spectrum is modeled well as the sum of only eight Gaussians – i.e., 24 parameters. We therefore limit the number of variables in this lineshape-fitting process by assuming the following:

(1) As for model 1, a statistical distribution of Al and Si cations, subject only to site occupancies g_i and a degree of aluminum avoidance described by α.

(2) For each site T_i, evenly spaced Si(k Al) peaks separated by a chemical shift increment $(\Delta\delta)_i$.

(3) For each site T_i, a single full-width at half-maximum w_i for all five Si(k Al) peaks.

These assumptions reduce the number of variables to 13: a value of g_i, $[\delta(0\,\mathrm{Al})]_i$, $(\Delta\delta)_i$, and w_i for $i = 1$–3, plus α. Even so, we have proceeded carefully in the simulation process to avoid wandering aimlessly through parameter space. Two different programs are used to iteratively minimize the least-squares difference between simulated and experimental lineshapes: one is based on subroutine POWELL (Press et al. 1986), the other on subroutine E04DBF from the Numerical Algorithms Group library.

Starting with trial lineshapes based on model 1 g_i values and chemical shift estimates from Table 4, we carry out the minimization in several stages. In the first stage, natural, heat-treated, and gel-synthesized leucite spectra have been fit simultaneously, with the same set of chemical shift and peak width parameters for each, and with R values constrained to be 2.06, 2.06, and 2.09 respectively. The common set of chemical shifts is to ensure that the three simulations remain mutually consistent. In later stages, to fine-tune the

Table 8. Model 3 simulation values for Al site occupancies and Si chemical shifts in leucite

Sample	Site	g_i	$[\delta(0\text{Al})]_i$ (ppm)	$(\Delta\delta)_i$ (ppm)	w_i (ppm)	R	α	Relative error (%)
Natural leucite	T_1	0.39	−108.6	5.17	4.3	2.09	0.0	6.9
	T_2	0.16	−101.5	4.58	3.5			
	T_3	0.42	− 93.8	4.26	3.1			
Heat-treated leucite	T_1	0.37	−108.4	5.02	3.9	2.11	0.11	6.3
	T_2	0.20	−101.2	4.56	3.5			
	T_3	0.41	− 93.5	4.17	2.9			
Gel-synthesized leucite	T_1	0.36	−108.0	4.79	3.8	2.07	0.0	6.0
	T_2	0.20	−100.8	4.27	3.3			
	T_3	0.42	− 94.0	4.31	3.0			
Roccamonfina leucite	T_1	0.40	−108.0	4.94	3.8	2.05	0.0	7.7
	T_2	0.15	−100.8	4.32	3.4			
	T_3	0.43	− 93.6	4.15	2.9			
Mt. Cimini leucite	T_1	0.38	−108.9	5.30	4.6	2.12	0.0	7.2
	T_2	0.16	−101.8	4.68	3.6			
	T_3	0.42	− 93.9	4.34	3.2			

fit, each spectrum is allowed to evolve separately and R is allowed to vary.

Results for the three aforementioned spectra are displayed in Figures 4–6 and listed in Table 8. Also in Table 8 are separate analyses for (unheated) Mt. Cimini and Roccamonfina leucite. Aluminum-occupancy values agree reasonably well with model 1 and model 2 data – the basic findings that $g_2 < g_1 \lesssim g_3$ and $\alpha \approx 0$ appear to be model independent. (The errors reported in Table 8, however, cannot be directly compared with those in Tables 6 and 7.) We note also that the Mt. Cimini and Roccamonfina distributions are indeed nearly identical (and hence nearly identical to the distribution calculated for their combined spectrum).

The chemical shifts calculated for the center peak of each site subspectrum, the $T_i(2\text{Al})$ silicons, match the estimates in Table 4 that are based on the Ramdas and Klinowski formula. However, the peak-to-peak chemical shift increments generated by model 3 are smaller than predicted values; for natural leucite, as an example, the differences are 0.26, 0.90, and 1.29 ppm for sites T_1, T_2, and T_3 respectively.

For every spectral simulation except that of heat-treated Mt. Cimini leucite, we find that when R and α are allowed to vary freely, R winds up close to the value expected from chemical analysis and α is zero: an apparent affirmation of Loewenstein's rule. The simulation for heat-treated leucite, when taken to completion, also yields $\alpha = 0$, but $R = 2.20$. When R is constrained to be more in line with chemical analysis ($R = 2.11$), then $\alpha = 0.11$. As noted earlier, a similar number is obtained using model 1. This result suggests that to some extent, silicon-aluminum reordering occurred in the sample during its week at 1673 K and a non-equilibrium distribution of cations was frozen out. We again caution, however, that the rms fit of a leucite simulation is rather insensitive to simultaneous variation of R and α.

What of the small differences between experimental lineshapes and model 3 simulations? To explore if these can be reduced, we have modified a model 3 program to minimize the number of electrostatically unfavorable Al–Si–Al linkages in accord with Dempsey's rule. Following Vega (1983), we count the number of such linkages by considering, for a given silicon, the number of ways n_D of selecting k Al neighbors two at a time: $n_D = 0$, 0, 1, 3, 6 for $k = 0$, 1, 2, 3, 4. The probability associated with each $T_i(k\text{ Al})$ Si species is modified by subtracting the quantity $(1 - g_i)\beta n_D$ and then renormalizing, where β is a Dempsey's rule parameter. In running simulations, however, we find that β is very small and changes sign from one leucite spectrum to another, suggesting that Dempsey's rule is not a driving force for the distribution of Si and Al in leucite.

Finally, we note that a "model 4" incorporating directed-jump intensities with full lineshape simulation would allow us to further investigate distributional constraints in leucite, but it is too computationally intensive for current use.

Comparison with ^{27}Al results

Phillips and Kirkpatrick (1986) have recently analyzed the ^{27}Al MAS NMR spectrum of leucite at 11.7 T, using spinning sideband analysis to resolve three peaks centered at 60.7, 63.9, and 68.7 ppm relative to aqueous $Al(H_2O)_6^{3+}$. Based on the bond angles of Mazzi et al. (1976), they assign these to T_1, T_2, and T_3 silicons respectively. The relative intensities appear to be equal, suggesting that $g_1 \simeq g_2 \simeq g_3$. Clearly, this finding is at odds with our data, but we have no ready explanation for the discrepancy.

Analysis of the Analcite Spectrum

Model 1 and model 2 simulations were also run to fit the peak areas listed in Table 2 for analcite. As noted earlier, because of the lack of an intrinsic site shift, each peak in the spectrum corresponds to a particular value of k, the number of Al neighbors. The symmetry is assumed to be tetragonal $I4_1/acd$ or very nearly so; as a consequence, sites T_1 and T_3 are equivalent and g_1 should equal g_3. Our results appear in Table 9. Both models find that two distinctly different Si, Al distributions give rise to minimal rms error values. In what we will call distribution A, aluminum cations are concentrated in the T_2 sites: $g_2 = 0.76$–0.78. In distribution B, almost all Al cations occupy $T_1 = T_3$ sites: $g_2 = 0.02$–0.04. (In contrast, constraining the three g_i values

Table 9. Model 1 and model 2 simulation values for the aluminum T_i site occupancies in analcite

Model	Distribution	Si/Al ratio	g_1	g_2	g_3	Relative rms error (%)
1	A	2.13	0.10	0.76	0.10	2.5
1	B	2.13	0.47	0.02	0.47	5.6
2	A	2.15	0.08	0.79	0.08	1.7
2	B	2.15	0.46	0.04	0.45	3.0

to be equal maximizes the rms error.) As in leucite, Loewenstein's rule appears to be valid; for both distributions, α goes to zero when allowed to vary freely. Moreover, there is evidence of a small Dempsey's rule effect: $\beta = 1.5 \times 10^{-3}$ for distribution A and 4.3×10^{-3} for distribution B.

It is impossible to choose between the two distributional models on the basis of our analcite NMR data alone. Had the potassium-exchanged analcite sample yielded a measurable spectrum, the ambiguity could be resolved using the extra information provided by intrinsic T_i chemical shifts. Alternatively, Mazzi and Galli (1978) have correlated aluminum occupancy with unit-cell dimensions: g_2 is proportional to the unit-cell edge along the c-axis; $g_1 = g_3$ is proportional to the unit-cell edge along the a-axis. A careful single-crystal x-ray determination of the unit-cell dimensions in our analcite sample should therefore allow us to select the correct distribution.

This measurement has not yet been made. We should note, however, that Mazzi and Galli proposed no value of g_2 higher than 0.50 for the seven analcite samples they analyzed. In addition, these authors developed several models for ordering in analcite that minimize electrostatic charge on framework oxygens by correlating g_i values with the occupancy of sodium ions in adjacent S sites. Their simplest model (Galli et al. 1978), that the Al fraction in a T_i site is half the adjacent Na occupancy, yields a maximum g_2 value of 0.5. A more detailed analysis (Mazzi and Galli 1978) relates the Na occupancy to $0.75(g_2) + 5/12$, for which the maximum g_2 value is 7/9 or approximately 0.778. When the effect of water molecules is included to better fit their experimental data, the maximum g_2 value becomes 0.6. Only the second of these models is compatible with distribution A.

Conclusions

As has been demonstrated previously in the study of zeolites, ^{29}Si magic-angle-spinning NMR spectroscopy can provide detailed information on silicon-aluminum ordering in minerals. On the basis of our data and the three distributional models we have investigated, we can conclude the following:

(1) Contrary to interpretations based on single-crystal x-ray work, the Si, Al distribution in leucite is not purely random: aluminum occupancy fractions for the three T_i sites are distinctly different. Distribution model 1 (random arrangement of Al cations subject to T_i site preferences and Loewenstein's aluminum-avoidance effect) yields $g_1 = 0.41$, $g_2 = 0.09$, and $g_3 = 0.50$ for a Mt. Cimini/Roccamonfina sample. Model 2 (directed "Loewensteinian" jumping of Al cations on a lattice of tetrahedral sites) generates a similar set of values: $g_1 = 0.37$, $g_2 = 0.14$, and $g_3 = 0.48$. Model 3 (lineshape simulation) yields $g_1 = 0.39$, $g_2 = 0.16$, and $g_3 = 0.42$.

A change in the Si, Al distribution is not likely to be involved in the rapid transition to the high-temperature form of leucite. Thus, as in other tectosilicates such as nepheline, some kind of long-range disorder of small, ordered domains is probably necessary to explain the long-range (XRD) cubic symmetry of this phase. The contribution of the observed ordering to the configurational entropy of leucite is small, but significant. Tabulated values of S^0_{298} (Robie et al. 1979) include a contribution of 15.88 J K^{-1} mol^{-1}, assuming complete Si, Al disorder. The range of site occupancies given above indicates that this value should be reduced to about 13.9–14.9 J K^{-1} mol^{-1}.

(2) Aluminum site preferences are nearly the same in natural and gel-synthesized leucite. They are, however, somewhat less pronounced in the synthetic sample, as one might expect for crystals that grew rapidly from a presumably disordered gel. Model 3 yields $g_1 = 0.36$, $g_2 = 0.20$, and $g_3 = 0.42$.

(3) For all samples except the heat-treated leucite, simulations indicate that there are essentially no Al–O–Al linkages.

(4) Heat treatment of the Mt. Cimini leucite sample at 1673 K for a week (which modifies its tetragonal-cubic phase transition) has no major effect on the short-range Si, Al distribution, but some rearrangement of Si and Al cations may occur. Model 1 and model 3 data suggest that after heat treatment, the number of Al–O–Al linkages present is roughly 10 percent of the number expected on a purely statistical basis.

On the whole, however, it seems to be true that aluminum avoidance is of general validity for tectosilicates in which Na or K is the primary charge-balancing cation. [An exception is ultramarine, the synthetic analog of lazurite: its aluminosilicate framework has been found to be completely disordered (Klinowski et al. 1987), but synthesis conditions suggest that the product is metastable.] The picture can be more complicated in systems with smaller or more highly charged interstitial cations. Silicon-29 MAS NMR results for synthetic, high-temperature cordierite ($Mg_2Al_4Si_5O_{18}$) indicate that substantial numbers of Al–O–Al linkages are present, but are removed via ordering that occurs during lower temperature annealing (Putnis et al. 1985; Putnis and Angel 1985). The symmetry of an unusual hexagonal polymorph of $CaAl_2Si_2O_8$, which crystallizes from a supercooled melt at extreme undercoolings (Davis and Tuttle 1952; Takeuchi and Donnay 1959), suggests that either local or domain disorder is greater than that found in the triclinic phase produced closer to equilibrium.

An explanation for this compositional effect probably lies in the greater strength of interaction between doubly charged (or small) interstitial cations with bridging oxygens, relative to that of singly charged (or large) cations. This interaction should help to stabilize Al–O–Al linkages, allowing more disorder in alkaline earth aluminosilicates than in alkali aluminosilicates. A similar effect in aluminosilicate melts may possibly be indicated by the fact that the ^{29}Si MAS NMR linewidth (a measure of disorder) observed in $CaAl_2Si_2O_8$ glass is much greater than that in $NaAlSiO_4$ glass (Murdoch et al. 1985).

(5) In fitting the experimental peak areas of analcite, both model 1 and model 2 simulations generate two dis-

tinctly different distributions A and B, the former with aluminum predominantly in T_2 sites ($g_1 = g_3 \approx 0.09$, $g_2 \approx 0.78$), the latter with only a scattering of T_2 Al cations ($g_1 = g_3 \approx 0.46$, $g_2 \approx 0.04$). A choice between distributions A and B could likely be made based on the spectrum of a K-exchanged sample or the unit-cell dimensions.

The detailed information on silicon-aluminum ordering in tectosilicates that can be obtained with ^{29}Si (and ^{27}Al) MAS NMR has been of great use in the design of zeolite catalysts for the chemical industry. Petrologic applications remain largely for future work but are potentially wide: cation distributions often reflect the geologically important variables of time, temperature, and composition. The ordering state of feldspar, as determined by x-ray diffraction and optical means, is an often-used clue to the temperature of ordering and to growth kinetics. Similar constraints on geochemical processes may be obtainable from studies of natural zeolites and feldspathoids. As a small start, we have shown here that leucite phenocrysts from very similar lavas of the Roman province are structurally nearly identical, but that material from the groundmass of a wyomingite lava is qualitatively different.

In short, now that the analytical tools have been developed, opportunities for future work include a more thorough investigation of Si, Al ordering in a variety of leucite minerals of different origin and thermal history. Ion exchange (with the inclusion of paramagnetic impurities to facilitate relaxation) will allow the direct comparison of distributional results from leucite-like and analcite-like spectra: one with and the other without intrinsic T_i site chemical shifts. Finally, the calibration of ordering with experimentally determined temperature and time of synthesis may provide new quantitative data on the origin of these types of minerals in nature.

Acknowledgments. Special thanks are due R. Lange for supplying the gel-synthesized leucite sample. We also thank B. Mysen for sending us a copy of the Raman lineshape-fitting program that we modified for NMR analysis, and the reviewers for their thoughtful (and thought-inducing) comments. This work was supported by the Director, Office of Basic Energy Sciences, Division of Engineering, Mathematics, and Geosciences of the U.S. Department of Energy under contract DEACO3-76SF00098; and by the National Science Foundation, grant number EAR-8507925.

References

Abragam A (1961) The Principles of Nuclear Magnetism. Oxford University Press, London

Barron PF, Frost RL, Skjemstad JO (1983) ^{29}Si spin-lattice relaxation in aluminosilicates. J Chem Soc Chem Commun: 581–583

Beger RM (1969) The crystal structure and chemical composition of pollucite. Z Kristallogr 129:280–302

Carmichael ISE (1967) The mineralogy and petrology of the volcanic rocks from the Leucite Hills, Wyoming. Contrib Mineral Petrol 15:24–66

Davis GL, Tuttle OF (1952) Two new crystalline phases of the anorthite composition, $CaO-Al_2O_3-2SiO_2$. Am J Science Bowen Volume: 107–114

Dempsey E, Kuhl GH, Olsen DH (1969) Variation of the lattice parameter with aluminum content in synthetic sodium faujasites. Evidence for ordering of the framework cations. J Chem Phys. 73:387–390

Ferraris G, Jones DW, Yerkess J (1972) A neutron-diffraction study of the crystal structure of analcime, $NaAlSi_2O_6 \cdot H_2O$. Z Kristallogr 135:240–252

Fyfe CA, Thomas JM, Klinowski J, Gobbi GC (1983) Magic-angle-spinning NMR (MAS-NMR) spectroscopy and the structure of zeolites. Angew Chem Int Ed Engl 22:259–275

Galli E, Gottardi G, Mazzi F (1978) The natural and synthetic phases with the leucite framework. Miner Petrogr Acta 22:185–193

Hamilton DL, Henderson CMB (1968) The preparation of silicate compositions by a gelling method. Mineral Mag 36:832–838

Jarman RH, Jacobson AJ, Melchior MT (1984) Interpretation of the silicon-29 nuclear magnetic resonance spectra of zeolites: synthetic mazzite. J Phys Chem 88:5748–5752

Klinowski J, Anderson MW (1986) A high-resolution solid-state nuclear magnetic resonance study of the ordering of silicon and aluminium in synthetic mazzite (zeolite omega). J Chem Soc Faraday Trans 1 82:569–584

Klinowski J, Carr SW, Tarling SE, Barnes P (1987) The aluminosilicate framework of ultramarine is completely disordered: a magic-angle-spinning NMR study. Nature, in press

Klinowski J, Ramdas S, Thomas JM (1982) A re-examination of Si, Al ordering in zeolites NaX and NaY. J Chem Soc Faraday Trans 2 78:1025–1050

Lange R, Carmichael ISE, Stebbins JF (1986) Phase transitions in leucite ($KAlSi_2O_6$), orthorhombic $KAlSiO_4$, and their iron analogs ($KFeSi_2O_6$, $KFeSiO_4$). Am Mineral 71:937–945

Lippmaa E, Magi M, Samoson A, Engelhardt G, Grimmer AR (1980) Structural studies of silicates by solid-state high-resolution ^{29}Si NMR. J Am Chem Soc 102:4889–4893

Lippmaa E, Magi M, Samoson A, Tarmak M, Engelhardt G (1981) Investigation of the structure of zeolites by solid-state high-resolution ^{29}Si NMR spectroscopy. J Am Chem Soc 103:4992–4996

Loewenstein W (1954) The distribution of aluminum in the tetrahedra of silicates and aluminates. Am Mineral 39:92–96

Mazzi F, Galli E (1978) Is each analcime different? Am Mineral 63:448–460

Mazzi F, Galli E, Gottardi G (1976) The crystal structure of tetragonal leucite. Am Mineral 61:108–115

Merlino S (1984) Feldspathoids: their average and real structure. In: Brown WL (ed) Feldspars and Feldspathoids (NATO Advanced Study Institute). Reidel Publishing Co, New York, pp 435–470

Murdoch JB, Stebbins JF, Carmichael ISE (1984) Silicon-29 MAS nuclear magnetic resonance study of the structure of feldspathoid minerals. Geol Soc Am Abst w Prog 16, 6:604

Murdoch JB, Stebbins JF, Carmichael ISE (1985) High-resolution ^{29}Si NMR study of silicate and aluminosilicate glasses: the effect of network-modifying cations. Am Mineral 70:332–343

Peacor DR (1968) A high temperature single crystal diffractometer study of leucite, $(K, Na)AlSi_2O_6$. Z Kristallogr 127:213–224

Phillips BL, Kirkpatrick RJ (1986) Increased resolution for solid-state ^{27}Al NMR. Abstracts, Fourteenth General Meeting of the International Mineralogical Association 198–199

Press WH, Flannery BP, Teukolsky SA, Vetterling WT (1986) Numerical Recipes: The Art of Scientific Computing. Cambridge University Press, Cambridge

Putnis A, Fyfe CA, Gobbi GC (1985) Al, Si ordering in cordierite using "magic angle spinning" NMR. I. Si^{29} spectra of synthetic cordierites. Phys Chem Minerals 12:211–216

Putnis A, Angel RJ (1985) Al, Si ordering in cordierite using "magic angle spinning" NMR. II. Models of Al, Si order from NMR data. Phys Chem Minerals 12:217–222

Ramdas S, Klinowski J (1984) A simple correlation between isotropic ^{29}Si-NMR chemical shifts and T–O–T angles in zeolite frameworks. Nature 308:521–523

Robie RA, Hemingway BS, Fisher JR (1979) Thermodynamic properties of minerals and related substances at 298.15 K and 1 bar (10^5 pascals) pressure and at higher temperatures. US Geol Survey Bull 1452

Schneider E, Stebbins JF, Pines A (1987) Speciation and local structure in alkali and alkaline earth silicate glasses: constraints from Si-29 NMR spectroscopy. J Non-Cryst Solids 89:371–383

Smith JV (1982) Geometrical and structural crystallography. Wiley, New York
Smith JV, Blackwell CS (1983) Nuclear magnetic resonance of silica polymorphs. Nature 303:223–225
Stebbins JF, Murdoch JB, Carmichael ISE, Pines A (1986) Defects and short-range order in nepheline group minerals: a silicon-29 nuclear magnetic resonance study. Phys Chem Minerals 13:371–381
Takeuchi Y, Donnay G (1959) The crystal structure of hexagonal $CaAl_2Si_2O_8$. Acta Crystallogr 12:465–470
Taylor WH (1930) The structure of analcite ($NaAlSi_2O_6 \cdot H_2O$). Z Kristallogr 74:1–19
Thomas JM, Klinowski J, Ramdas S, Hunter BK, Tennakoon DTB (1983) The evaluation of non-equivalent tetrahedral sites from ^{29}Si NMR chemical shifts in zeolites and related aluminosilicates. Chem Phys Lett 102:158–162
Vega AJ (1983) A statistical approach to the interpretation of silicon-29 NMR of zeolites. In: Stucky GD, Dwyer FG (eds) Intrazeolite Chemistry. American Chemical Society, Washington, D.C., pp 217–230
Waldbaum DR, Robie RA (1971) Calorimetric investigation of Na–K mixing and polymorphism in the alkali feldspars. Z Kristallogr 184:381–420

Received October 9, 1986

Note added in proof. Brown et al. (1987) have recently presented ^{29}Si MAS NMR spectra of natural and synthetic leucite that are very similar to those displayed here. They have also simulated these lineshapes using chemical shifts derived from the empirical secant rule of Smith and Blackwell (1983) with a reasonable choice for individual peak widths. By varying only the Al distribution among T_i sites (but assuming an otherwise random arrangement of Al and Si), they find $g_1 = 0.56$, $g_2 = 0.36$, and $g_3 = 0.08$. These values differ from ours primarily in that the effect of aluminum avoidance was not considered.

Brown IWM, Cardile CM, MacKenzie KJD, Ryan MJ, Meinhold RH (1987) Natural and synthetic leucites studied by solid state ^{29}Si and ^{27}Al NMR and ^{57}Fe Mossbauer spectroscopy. Phys Chem Minerals 15:78–83